ARTICLE OPEN

Check for updates

ErbB inhibition rescues nigral dopamine neuron hyperactivity and repetitive behaviors in a mouse model of fragile X syndrome

Sebastian L. D'Addario[1], Eleonora Rosina[2], Mariangela Massaro Cenere[1], Claudia Bagni[2,3], Nicola B. Mercuri[1,4] and Ada Ledonne[1,5]✉

Repetitive stereotyped behaviors are core symptoms of autism spectrum disorders (ASD) and fragile X syndrome (FXS), the prevalent genetic cause of intellectual disability and autism. The nigrostriatal dopamine (DA) circuit rules movement and creation of habits and sequential behaviors; therefore, its dysregulation could promote autistic repetitive behaviors. Nevertheless, inspection of substantia nigra pars compacta (SNpc) DA neurons in ASD models has been overlooked and specific evidence of their altered activity in ASD and FXS is absent. Here, we show that hyperactivity of SNpc DA neurons is an early feature of FXS. The underlying mechanism relies on an interplay between metabotropic glutamate receptor 1 (mGluR1) and ErbB tyrosine kinases, receptors for the neurotrophic and differentiation factors known as neuregulins. Up-regulation of ErbB4 and ErbB2 in nigral DA neurons drives neuronal hyperactivity and repetitive behaviors of the FXS mouse, concurrently rescued by ErbB inhibition. In conclusion, beyond providing the first evidence that nigral DA neuron hyperactivity is a signature of FXS and nigral mGluR1 and ErbB4/2 play a relevant role in FXS etiology, we demonstrate that inhibiting ErbB is a valuable pharmacological approach to attenuate stereotyped repetitive behaviors, thus opening an avenue toward innovative therapies for ASD and FXS treatment.

Molecular Psychiatry; https://doi.org/10.1038/s41380-024-02831-y

INTRODUCTION

Repetitive behaviors, such as stereotyped movements, repetitive objects handling, and self-injurious behaviors, are core diagnostic signs of autism spectrum disorders (ASD), also overt in fragile X syndrome (FXS), the main genetic cause of autism and intellectual disability caused by *Fmr1* silencing and loss of Fragile X Messenger Ribonucleoprotein (FMRP) [1–3]. The nigrostriatal dopamine (DA) circuit, arising from DA neurons of the substantia nigra pars compacta (SNpc), is key to movement control and the creation of habits and sequential behaviors [4, 5]; thus, its dysregulation is posited as a leading substrate of abnormal movements and restricted routines, emerging as compulsive and stereotyped behaviors in patients with ASD and FXS. Earlier clues about the role of the SNpc DA nucleus in repetitive behaviors stand up from evidence that pharmacological and genetic manipulations increasing striatal DA transmission in rodents promote stereotyped movements by striatal D1 activation [6–11]. The latest demonstration that optogenetic activation of SNpc DA neurons triggers self-grooming (a repetitive behavior) in mice [12] and self-grooming is attenuated by optogenetic inhibition of the SNpc-to-ventromedial striatum circuit [13] has strengthened the idea that hyperactivation of the nigrostriatal DA circuit is instrumental for repetitive behaviors. However, so far, precise evidence proving altered activity of nigral DA neuron in ASD or FXS models is absent, keeping the involvement of the SNpc DA nucleus in abnormal repetitive behaviors in ASD still rather theoretical [14–17].

Striatal dysfunctions have been recently reported in the *Fmr1* KO mouse, a validated model for FXS [18, 19]. Few other studies described histological and neurochemical DA alterations in the striatum of this FXS model [17]: evidence is partially divergent, as histological analyses of the nigrostriatal DA circuit in adult *Fmr1* KO mice found increased branching of striatal tyrosine hydroxylase positive (TH+) terminals [20] or loss of SNpc DA neurons [21], while evaluation of striatal DA dynamics reported bidirectional age-dependent changes in this FXS model, with higher DA turnover at one month [22], increased DA tissue levels at two months [23], and a reduction of basal levels [24] and electrically-evoked DA release [25] in older mice. Due to these disjointed data and, more importantly, shortage of direct investigation of nigral DA neuron activity in ASD and FXS models, current knowledge about the role of the nigrostriatal DA circuit in ASD and FXS is inadequate. Furthermore, since evidence of striatal DA alterations in FXS models is mostly restricted to adulthood, the earlier DA-dependent mechanisms driving pediatric FXS symptoms are entirely unknown.

In the present study, we directly assess whether the nigrostriatal DA circuit contributes to the etiological processes of FXS by

[1]Department of Experimental Neuroscience, Santa Lucia Foundation IRCCS, Rome, Italy. [2]Department of Biomedicine and Prevention, University of Rome Tor Vergata, Rome, Italy. [3]Department of Fundamental Neurosciences, University of Lausanne, Lausanne, Switzerland. [4]Neurology Unit, Department of Systems Medicine, University of Rome Tor Vergata, Rome, Italy. [5]Pharmacology Unit, Department of Systems Medicine, University of Rome Tor Vergata, Rome, Italy. ✉email: adaledonne@gmail.com

Received: 16 April 2024 Revised: 2 November 2024 Accepted: 5 November 2024
Published online: 15 November 2024

analyzing the activity of nigral DA neurons in adolescent *Fmr1* KO mice. We show that hyperactivity of nigral DA neurons is an early signature of FXS, and the underlying mechanism relies on the interaction between metabotropic glutamate receptor 1 (mGluR1) and ErbB tyrosine kinases, receptors for the neurotrophic and differentiation factors known as neuregulins (NRGs). Lastly, we investigate whether pharmacological inhibition of ErbB signaling represents a valuable approach to rescue nigral DA neuron dysfunctions and repetitive behaviors in the FXS model.

MATERIALS AND METHODS

Detailed methodological information is provided in the Supplementary Material.

Mice

All procedures were conducted according to the guidelines on the ethical use of animals from the Council Directive of the European Communities (2010/63/EU) and were approved by the Italian Ministry of Health (authorization N°143-2020PR). *Fmr1* KO mice (C57/BL6J background) and C57/BL6J wild-type (WT) mice were obtained from Jackson Laboratories (USA) and then bred in our facility in a temperature- and humidity-controlled environment with a 12 h light/dark cycle. All experiments were performed in adolescent male mice of 21–34 days of age.

In vivo pharmacological treatments

Stereotaxic surgery and intracerebral drug injections. Mice (P26-28) were anaesthetized and bilaterally implanted with a guide cannula above the SNpc (AP: −3.4, ML: 1.2, DV: −3.6 mm) [26]. After recovery (4–6 days), mice were injected with the ErbB inhibitor PD158780 (10 µM) or it vehicle (0.1% DMSO in aCSF) through a microinfusion system (0.6 µl/side, 0.3 µl/min). After 30 min, mice were used for electrophysiological or behavioral experiments.

Systemic drug injections. Mice (P30-32) were injected intraperitoneally with PD158780 (10 mg/Kg) or vehicle (30% DMSO in NaCl 0.9%) and after one hour were used for electrophysiological or behavioral analyses.

The pharmacological treatments were designed based on our previous evidence [27, 28] and other studies [29].

Midbrain slice preparation

Midbrain slices containing the SNpc were used for electrophysiology, immunofluorescence, and SNpc microdissections for western blots. Midbrain slices were obtained as previously reported [30]; details are provided in the Supplementary Material.

Electrophysiology

Detailed information is reported in the Supplementary Material. Patch-clamp recordings of SNpc DA neurons were performed with pipettes filled with (in mM): 125 K-gluconate, 10 KCl, 10 HEPES, 2 $MgCl_2$, 4 ATP-Mg, 0.3 GTP-Na, 0.75 EGTA, 0.1 $CaCl_2$, 10 Phosphocreatine-Na_2. The spontaneous firing activity was recorded in cell-attached or whole-cell configuration. Membrane resistance (R_m) and capacitance (C_m) were measured with the "membrane test" protocol (Clampex) [27, 31]. Nigral DA neuron excitability was evaluated by injection of depolarizing currents (+50/+250 pA, $V_H = -60$ mV) and quantification of evoked action potentials. Excitation/Inhibition (E/I) balance in single DA neurons was estimated by recording spontaneous excitatory postsynaptic currents (sEPSCs) ($V_H = -70$ mV) and spontaneous inhibitory postsynaptic currents (sIPSCs) ($V_H = +10$ mV) in presence of AMPARs- and NMDARs antagonists with pipettes filled with (in mM) 115 Cs-methanesulfonate, 10 CsCl, 0.45 $CaCl_2$, 10 HEPES, 1 EGTA, 5 QX-314, 4 ATP-Mg, 0.3 GTP-Na. The mGluR1/5 agonist (S)-DHPG (10 µM) was used to evoke mGluR1/5-activated currents (I_{DHPG}); mGluR5- or mGluR1-activated currents were isolated with the mGluR1 antagonist CPCCOEt or the mGluR5 antagonist MPEP, respectively [27]. For acute ErbB inhibition, PD158780 (10 µM) was perfused on SNpc slices for 20-25 min. For in vivo intra-SNpc ErbB inhibition, PD158780 (10 µM, 0.6 µL) or its vehicle (0.1% DMSO in aCSF) were injected in SNpc 30 min before starting procedures for patch-clamp recordings. For systemic ErbB inhibition, PD158780 (10 mg/Kg) or its vehicle (30% DMSO in NaCl 0.9%) were intraperitoneally injected 1 h before procedures for patch-clamp recordings.

Western blots

SNpc and VTA were dissected from midbrain slices of 25-day-old *Fmr1* KO and WT mice following published procedures [27, 30]. Detailed methodological information about sample preparation, western blots and quantification of mGluR1, ErbB4, ErbB2, and NRG1 levels is provided in the Supplementary Material.

Immunofluorescence and densitometric analysis

Midbrain slices of 25-day-old *Fmr1* KO and WT mice were used for immunofluorescence and densitometric analyses of mGluR1, ErbB4, and ErbB2 within nigral DA neurons. Details are reported in the Supplementary Material.

Behavior

All behavioral tests were conducted between 9:00 am and 16:00 pm after 1 h of room acclimation.

Analyses of repetitive behaviors. A mouse was placed in an empty cage (24 × 13 × 20 cm) filled with fresh home-bedding for 15 min. After 5 min of habituation, mice were inspected for repetitive behaviors by an observer evaluating time spent in self-grooming or digging, and jumping number.

Marble burying test. Marble burying test was conducted following published procedures [32] with minor modifications. A mouse was placed in a clean cage (40 ×18 × 26 cm) filled with fresh home-bedding (5 cm) and containing 20 marbles. After 30 min of freely exploration, marbles buried were counted by considering buried a marble covered ≥ 50% with bedding.

Open field. A mouse was placed in a circular open field (60 cm diameter, 30 cm height) for 30 min for evaluation of locomotor activity [28]. Total distance moved was analysed using Ethovision XT17 software (Noldus).

Statistical analyses

For normally distributed data, comparisons were performed by two-tailed paired or unpaired Student's *t* test, two-way ANOVA, and repeated measures two-way ANOVA followed by post hoc tests. When normality was violated, data were analyzed with Mann–Whitney test or Kruskal-Wallis ANOVA followed by Kolmogorov-Smirnov test. Outliers were evaluated with the Grubbs test and excluded from analyses. Data are represented as mean ± SEM. Statistical significance was set at $p < 0.05$.

RESULTS

Hyperactivity of nigral dopamine neurons in a FXS model

To evaluate whether SNpc DA neuron activity is altered in FXS, we performed electrophysiological recordings in acute midbrain slices of male adolescent *Fmr1* KO and WT mice (Fig. 1a). First, we analyzed spontaneous firing activity in the patch clamp cell-attached configuration and observed that nigral DA neurons in the FXS mouse spontaneously fired action potentials (APs) at higher frequencies than WT (Fig. 1b). Analysis of the coefficient of variation of the interspike intervals (CV-ISIs) revealed a similar temporal distribution of spikes (Fig. 1c), supporting maintenance of pacemaker regularity despite increased firing rate. Nigral DA neuron hyperactivity was overt in the FXS mouse at postnatal days (PND) 21-23 (supplementary Fig. S1), and was also evident in the whole-cell mode (Fig. 1d). SNpc DA neurons from the FXS mouse also showed modifications in passive membrane properties, precisely increased cell capacitance (C_m) (Fig. 1e), but no changes in membrane resistance (R_m) (Fig. 1f). To verify variations in neuronal excitability, we measured APs evoked by depolarizing currents, revealing that SNpc DA neurons from *Fmr1* KO mice fired more APs than WT (Fig. 1g). Collectively, these data demonstrate early dysregulation of the nigrostriatal DA circuit in FXS, identifying SNpc DA neuron hyperactivity as a novel feature of FXS.

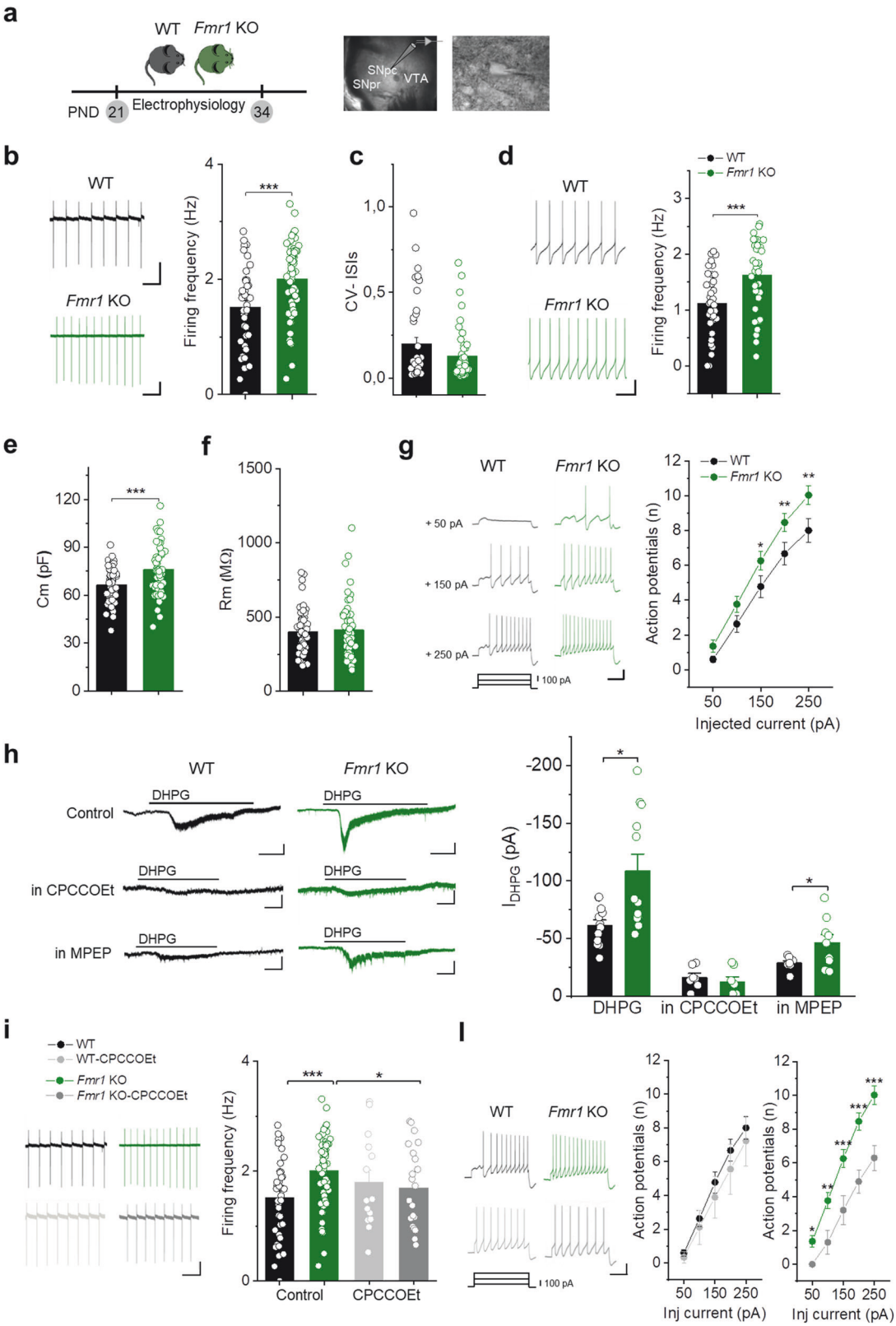

Abnormal mGluR1 function drives nigral DA neuron hyperactivity in the FXS mouse

The spontaneous firing activity of SNpc DA neurons is tightly controlled by several intrinsic and extrinsic factors that allow repetitive AP generation and pauses, resulting in tonic pacemaker activity in a narrow low-frequency range in ex vivo preparations [33]. In addition to intrinsic ion channels, afferent excitatory (E) and inhibitory (I) synaptic inputs can shape the firing rate. Since E/I imbalance is a common synaptic alteration underlying abnormal neuronal activity and circuitry connectivity in FXS [3, 34], we

Fig. 1 Hyperactivity of nigral dopamine neurons reliant on mGluR1 hyperfunction in a FXS model. a Left, schematic of ex vivo electrophysiological recordings of nigral dopamine (DA) neurons in adolescent mice. Middle, image of an horizontal slice displaying the recordings' site, the substantia nigra pars compacta (SNpc). Right, image of a SNpc DA neuron during the patch-clamp procedure. **b** Left, example firing traces in cell-attached mode. Right, plot of mean firing frequency showing increased firing rate of SNpc DA neurons from *Fmr1* KO (n = 59 cells/10 mice) compared with WT mice (n = 41 cells/8 mice); $p = 3.913 \times 10^{-4}$, two-tailed unpaired t test. Scale bar: 20 pA/1 s. **c** Plot of coefficient of variation of interspike intervals (CV-ISIs) in WT (n = 40 cells/8 mice) and *Fmr1* KO (n = 48 cells/10 mice), $p = 0.211$, Mann–Whitney test. **d** Left, example firing trace in whole-cell mode; Right, quantification of firing frequencies of WT (n = 36 cells/8 mice) and *Fmr1* KO mice (n = 38 cells/10 mice), $P = 3.037 \times 10^{-4}$, Mann–Whitney test. Scale bar: 20 mV/1 s. **e** Plot of membrane capacitance (C_m) and (**f**) membrane resistance (R_m) of nigral DA neurons from WT ($n = 50$ cells/8 mice) and *Fmr1* KO mice ($n = 53$ cells/10 mice). C*m*: $P = 4.87 \times 10^{-4}$, two-tailed unpaired t test; R_m: $p = 0.711$, two-tailed unpaired t test. Scale bar: 20 mV/1 s. **g** Left, example traces of action potentials (APs) evoked by current injections (holding voltage (V_H) = −60 mV) in nigral DA neurons; Right, APs number at each current step. WT (n = 27 cells/7 mice) and *Fmr1* KO mice (n = 39 cells/9 mice). RM two-way ANOVA followed by Tukey's test. Genotype: $p = 0.047$, Current $p = 1.76 \times 10^{-50}$, Genotype X Current $p = 0.095$. $p = 0.023$ at 150 pA, $p = 0.003$ at 200 pA; $p = 0.001$ at 250 pA. Scale bar: 25 mV/0.5 s. All data are presented as mean ± SEM. **h** Left, example traces of currents activated by the mGluR1/5 agonist DHPG (10 μM) (I_{DHPG}) in SNpc DA neurons in control and during mGluR1 or mGluR5 inhibition with CPCCOEt (100 μM) or MPEP (10 μM), respectively. Right, quantification of I_{DHPG} amplitudes showing increased I_{DHPG} in *Fmr1* KO mice (n = 12 cells/4 mice) compared with WT (n = 12 cells/3 mice). $p = 0.023$, Mann–Whitney test. I_{DHPG} potentiation in the FXS mouse depends selectively on mGluR1. I_{DHPG} in CPCCOEt: WT (n = 7 cells/3 mice) and *Fmr1* KO (n = 7 cells/3 mice), $p = 0.56$, two-tailed unpaired t test. I_{DHPG} in MPEP: WT (n = 8 cells/3 mice) and *Fmr1* KO (n = 9 cells/4 mice), $p = 0.041$, two-tailed unpaired t test. Scale bar: 20 pA/ 0.5 s. **i** Example spontaneous firing traces (left) and quantification of firing rates (right) showing that CPCCOEt attenuates SNpc DA neuron hyperactivity in the FXS mouse. WT-control (n = 41 cells/8 mice), *Fmr1* KO-control (n = 59 cells/10 mice), WT-CPCCOEt (n = 14 cells/5 mice), and *Fmr1* KO-CPCCOEt (n = 21 cells/5 mice). Two-way ANOVA followed by Fisher's test. Genotype x Drug $p = 0.026$. $p = 6.571 \times 10^{-4}$ for WT-control vs *Fmr1* KO-control, $p = 0.047$ for *Fmr1* KO-control vs *Fmr1* KO-CPCCOEt. Scale bar: 20 pA/1 s. **l** Example traces (left) and plots of APs number (right) showing that inhibiting mGluR1 reduces SNpc DA neuron hyperexcitability in the FXS mouse. RM two-way ANOVA followed by Tukey's test. CPCCOEt effect in WT: WT-control (n = 27 cells/7 mice) and WT-CPCCOEt (n = 9 cells/5 mice). Drug $P = 0.635$, Current $p = 1.331 \times 10^{-11}$, Drug X Current $p = 0.304$. CPCCOEt effect in *Fmr1* KO: *Fmr1* KO-control (n = 39 cells/10 mice) and *Fmr1* KO-CPCCOEt (n = 10 cells/5 mice). Drug $p = 0.002$, Current $p = 7.039 \times 10^{-17}$, Drug X Current $p = 0.0277$. $p = 0.045$ at 50 pA, $p = 0.001$ at 100 pA, $p = 1.063 \times 10^{-4}$ at 150 pA, $p = 2.230 \times 10^{-5}$ at 200 pA, $p = 8.657 \times 10^{-6}$ at 250 pA. Scale bar: 25 mV/0.5 s. All data are presented as mean ± SEM.

analyzed E/I ratio in nigral DA neurons by recording from the same neuron either spontaneous excitatory- (sEPSC, $V_H = -70$ mV) or inhibitory synaptic currents (sIPSC, $V_H = +10$ mV). We found no differences in frequency and amplitude of sEPSCs and sIPSCs (supplementary Fig. S2), indicating normal E/I balance of fast synaptic transmission in the FXS model. These findings exclude that changes in glutamate or GABA release are major determinants of nigral DA neuron hyperactivity in the FXS mouse.

Group I metabotropic glutamate receptors (mGluRI) — mGluR1 and mGluR5 — control essential brain functions, influencing neuronal activity, neurotransmission, and synaptic plasticity in several brain areas [35, 36]. While abnormal mGluR5 function is a recognized signature of FXS, the contribution of mGluR1 to FXS etiology is overlooked. As mGluR1 activation depolarizes SNpc DA neurons and enhances pacemaker and bursting firing [27, 37–39], we investigated whether mGluR1 hyperfunction is the functional substrate for nigral DA neuron hyperactivity in the FXS model. To test this, we first measured the depolarizing currents induced by the mGluR1/5 agonist DHPG (10 μM) (I_{DHPG}), revealing that I_{DHPG} is potentiated in the nigral DA neurons of the FXS mouse (Fig. 1h). I_{DHPG} analyses in the presence of selective antagonists demonstrated that I_{DHPG} enhancement relies exclusively on mGluR1; a pretreatment with the mGluR1 antagonist CPCCOEt (100 μM), but not with the mGluR5 antagonist MPEP (10 μM), occluded I_{DHPG} differences between genotypes (Fig. 1h). Next, we evaluated if an abnormal mGluR1 function drives hyperactivity and hyperexcitability of nigral DA neurons in the FXS model. Blunting mGluR1 activity normalized spontaneous firing frequency (Fig. 1i) and excitability (Fig. 1l) of SNpc DA neurons in the FXS mouse. These findings reveal an unrecognized contribution of mGluR1 to the neurobiological mechanisms of FXS, showing that mGluR1 hyperfunction triggers early hyperactivation of the nigrostriatal DA circuit.

Molecular determinants of mGluR1 hyperfunction

To assess whether mGluR1 hyperfunction in nigral DA neurons of the FXS mouse is associated with increased expression of mGluR1, we analyzed mGluR1 levels using the Western blot technique in homogenates of SNpc microdissected from 25-day-old adolescent mice (Fig. 2a). We found higher levels of nigral mGluR1 in the FXS mouse (Fig. 2b). Interestingly, such mGluR1 up-regulation appears confined to SNpc, since mGluR1 levels are unchanged in the adjacent DA nucleus, the ventral tegmental area (VTA) (supplementary Fig. S3).

What molecular event promotes mGluR1 up-regulation in the FXS mouse? We previously reported that the expression of mGluR1 in nigral DA neurons of wild-type rodents is regulated by ErbB tyrosine kinases, activated by the neurotrophic and differentiation factors neuregulins (NRGs) [27]. The NRGs family — including different types (NRG1-NRG6) and several splicing-derived isoforms — acts on homo- or heterodimeric receptors, composed of ErbB2, ErbB3, and ErbB4 subtypes [35]. ErbB4-ErbB4 and ErbB2-ErbB4 mediate NRGs/ErbB-induced effects on mGluR1 expression and function in SNpc DA neurons [27, 40]. Dysregulation of the NRGs/ErbB axis has been firstly associated with schizophrenia, based on studies identifying *Nrg1* and *ErbB4* as risk genes and evidence linking NRGs/ErbB alterations with schizophrenic symptoms [41–44]. Recently, *Nrg1* polymorphisms have also been reported in ASD [45, 46]; however, clinical evidence on NRG1 expression in the blood of patients with idiopathic ASD reported controversial data (describing increased [47, 48] or reduced levels [49]), thus the factual role of NRGs/ErbB signaling in ASD remains still elusive. Remarkably, NRGs/ErbB dysregulation has never been proposed in FXS.

Based on our previous evidence that ErbB stimulation promotes mGluR1 synthesis (Fig. 2c) and considering that ErbB4 and ErbB2 are listed as putative FMRP targets [50–53], we predicted that FMRP deficiency triggers ErbB4 and ErbB2 up-regulation in nigral DA neurons and, subsequently, abnormal ErbB signaling promotes mGluR1 overproduction and neuronal hyperactivity. To test this hypothesis, we first checked the expression of nigral ErbB4 and ErbB2, revealing a robust increase in ErbB4 levels (Fig. 2d) and a trend toward up-regulation of ErbB2 in the FXS model (Fig. 2e). Differently, NRG1 — the prototypical ErbB ligand — either in a full-length membrane-anchored form or as a cleaved soluble domain appeared normally expressed in the FXS mouse (Fig. 2f). Next, to demonstrate that up-regulations of mGluR1 and ErbB4/ErbB2 occur within nigral DA neurons, we quantified by immunofluorescence their optical densities in SNpc tyrosine hydroxylase positive (TH +) neurons. The results show increased expression of mGluR1 (Fig. 2g), ErbB4 (Fig. 2h), and ErbB2 (Fig. 2i) within nigral DA neurons in the FXS mouse.

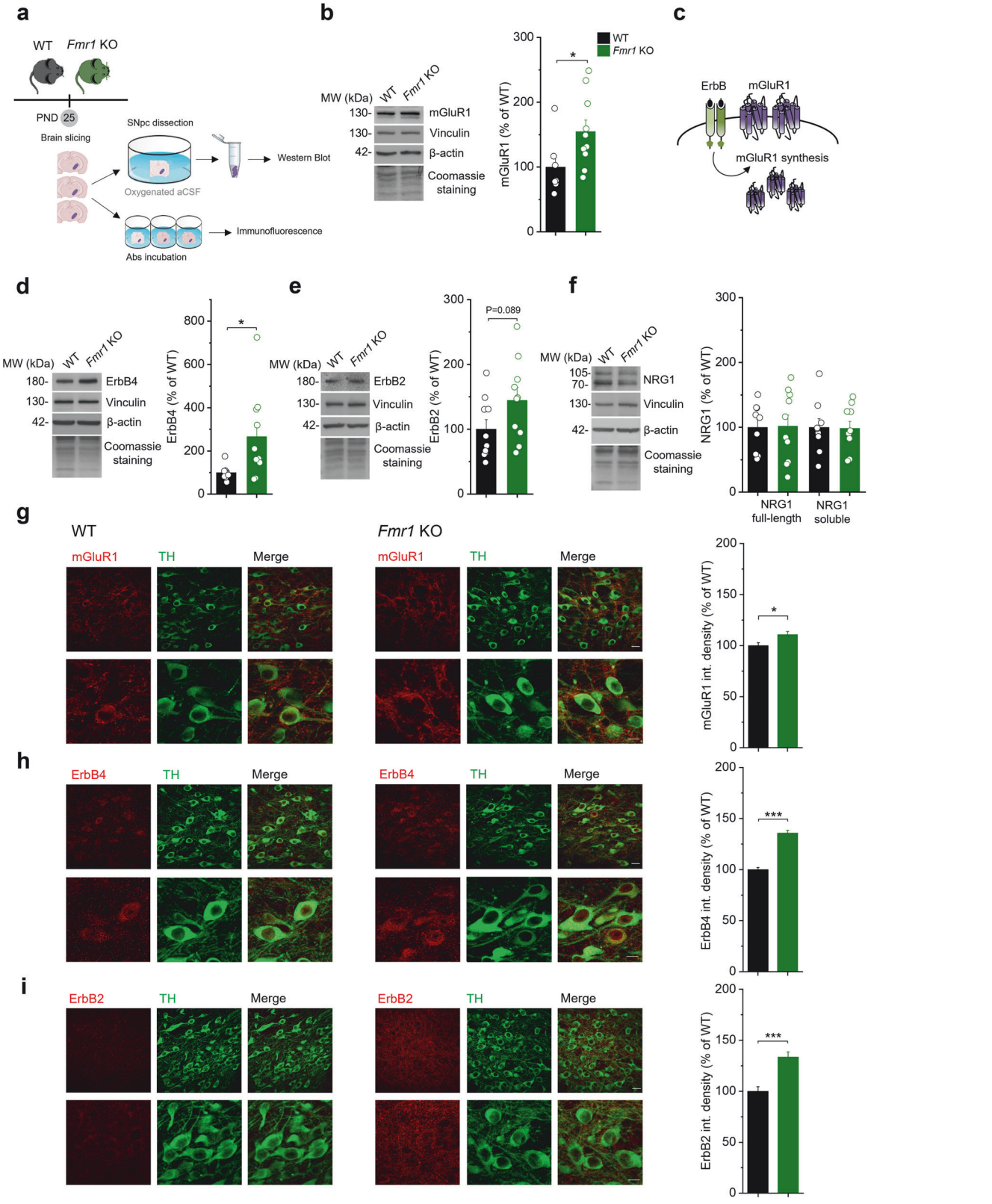

ErbB inhibition rescues nigral DA neuron dysfunctions in the FXS mouse

Next, we aimed to demonstrate that abnormal ErbB signaling drives mGluR1-dependent hyperactivity of SNpc DA neurons in the FXS mouse. Previously, we reported that tonic ErbB signaling shapes mGluR1 function in nigral DA neurons, by fine-tuning its membrane expression. The ErbB4 and ErbB2 inhibitor PD158780 hampers mGluR1 function by promoting receptor internalization [27, 35, 40] (Fig. 3a). Here, we tested whether ErbB inhibition can attenuate mGluR1 hyperfunction and rescue hyperactivity and

Fig. 2 Up-regulation of mGluR1, ErbB4, and ErbB2 in SNpc DA neurons of the FXS mouse. a Experimental pipeline for western blots and immunofluorescence experiments. **b** Left, cropped representative western blots showing mGluR1 protein levels in total SNpc from WT ($n = 7$) and *Fmr1* KO mice (n = 10). The molecular weight of each protein is indicated in kDa. Right, quantification of the western blots showing the signal intensity normalized over the WT (%) ($p = 0.018$, Mann–Whitney test). **c** Cartoon depicting ErbB-dependent regulation of mGluR1 synthesis and membrane trafficking in SNpc DA neurons [27]. **d** Left, cropped representative western blots showing ErbB4 protein levels in total SNpc from WT ($n = 9$) and *Fmr1* KO mice (n = 10). Right, quantification of the western blots normalized over the WT (%). ($p = 0.035$, Mann–Whitney test). **e** Left, cropped representative western blots showing ErbB2 protein levels in total SNpc from WT (n = 10) and *Fmr1* KO mice (n = 10). Right, quantification of the western blots normalized over the WT (%). ($p = 0.089$. Mann–Whitney test). **f** Left, cropped representative western blots showing NRG1 full-length and soluble forms protein levels in total SNpc from WT (n = 9) and *Fmr1* KO mice (n = 10). Right, quantification of the western blots normalized over the WT (%). (NRG1 full-length: $p = 0.983$; NRG1 soluble form: $p = 0.887$. Mann–Whitney test). **b, d–f** Data are presented as mean ± SEM. Protein levels were normalized to the average of Coomassie staining, vinculin and β-actin. **g** Left, double-labeled confocal images of mGluR1 (red) and tyrosine hydroxylase (TH) (green) in SNpc DA neurons captured at lower (up) and higher (bottom) magnification. Right, plot of mGluR1 integrated density (as % of WT) in nigral DA neurons of WT (n = 197 cells/3 mice) and *Fmr1* KO mice (n = 195 cells/3 mice). $p = 0.037$, Mann–Whitney test. **h** Left, double-labeled confocal images of ErbB4 (red) and TH (green). Right, quantification of ErbB4 integrated density (as % of WT) in SNpc DA neurons of WT (n = 257 cells/3 mice) and *Fmr1* KO (n = 392 cells/3 mice). $p = 8.71 \times 10^{-20}$, Mann–Whitney test. **i** Left, double-labeled confocal images of ErbB2 (red) and TH (green) in SNpc DA neurons. Right, plot of ErbB2 integrated density (as % of WT) in nigral DA neurons from *Fmr1* KO (n = 200 cells/3 mice) and WT mice (n = 179 cells/3 mice). $p = 1.859 \times 10^{-7}$, Mann–Whitney test. **g–i** Data are presented as mean ± SEM. Scale bar is 20 µm at lower magnification (up) and 10 µm at higher magnification (down).

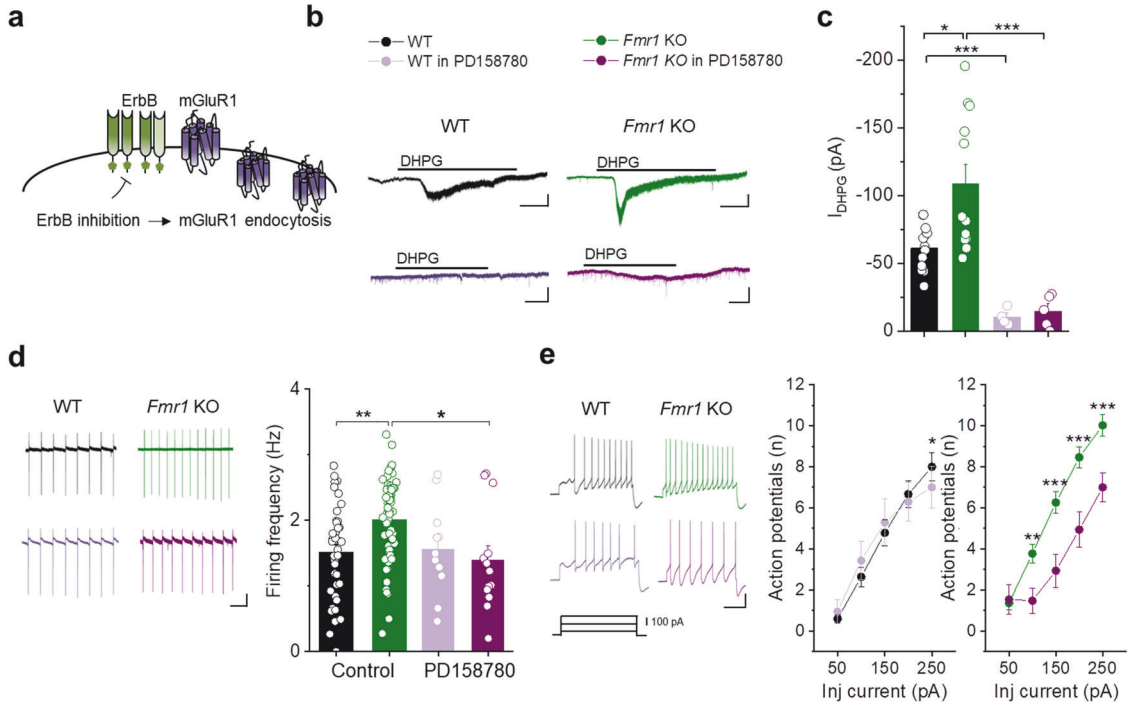

Fig. 3 ErbB inhibition offsets mGluR1-dependent hyperactivity of SNpc DA neurons in the FXS mouse. a Cartoon depicting ErbB inhibition induces mGluR1 endocytosis in SNpc DA neurons [27]. **b** Example I_{DHPG} traces in SNpc DA neurons in control and during treatment with PD158780 (10 µM). Scale bar: 20 pA/0.5 s. **c** Plot of I_{DHPG} amplitudes showing that ErbB inhibition reduces mGluR1 function in both genotypes. WT-control (n = 12 cells/3 mice), *Fmr1* KO-control ($n = 12$ cells/4 mice), WT-PD158780 (n = 4 cells/3 mice), and *Fmr1* KO-PD158780 (n = 5 cells/3 mice). Kruskall-Wallis ANOVA followed by Mann–Whitney test. ANOVA $p = 6.760 \times 10^{-5}$. $p = 0.020$ for WT-control vs *Fmr1* KO-control; $p = 0.0011$ for WT-control vs WT-PD158780; $p = 3.232 \times 10^{-4}$ for *Fmr1* KO-control vs *Fmr1* KO-PD158780. **d** Example firing traces (left) and quantification of firing frequency (right). WT-control (n = 41 cells/8 mice), *Fmr1* KO-control (n = 59 cells/10 mice), WT-PD158780 (n = 11 cells/6 mice), and *Fmr1* KO-PD158780 (n = 13 cells/6 mice). Two-way ANOVA followed by Tukey's test. Genotype x Drug $p = 0.0348$; $p = 0.002$ for WT vs *Fmr1* KO, $p = 0.015$ *Fmr1* KO vs *Fmr1* KO in PD158780. Scale bar: 20 pA/1 s. **e** Example traces (left) and plots (right) of evoked APs, showing that ErbB inhibition normalizes SNpc DA neuron hyperexcitability in the FXS mouse. PD158780 effect in WT: WT-control (n = 27 cells/7 mice) and WT-PD15870 (n = 14 cells/5 mice). RM two-way ANOVA followed by Tukey's test. Drug $p = 0.618$, Current $p = 7.413 \times 10^{-28}$, Drug X Current $p = 0.032$. $p = 0.0341$ at 250 pA. PD158780 effect in *Fmr1* KO: *Fmr1* KO-control (n = 39 cells/10 mice) and *Fmr1* KO-PD158780 (n = 15 cells/6 mice). Drug $p = 0.006$, Current $p = 1.271 \times 10^{-28}$, Drug x Current $p = 1.514 \times 10^{-4}$. $p = 0.003$ at 100 pA, $p = 1.735 \times 10^{-5}$ at 150 pA, $p = 1.089 \times 10^{-5}$ at 200 pA, $p = 6.825 \times 10^{-5}$ at 250 pA. Scale bar: 25 mV/0.5 s. All data are presented as mean ± SEM.

hyperexcitability of nigral DA neurons in the FXS mouse. We found that PD158780 (10 µM) reduced I_{DHPG} (Fig. 3b, c) and normalized spontaneous firing rate (Fig. 3d) and hyperexcitability (Fig. 3e) of nigral DA neurons of *Fmr1* KO mice. Collectively, these data support a causal link between amplified ErbB signaling, mGluR1 hyperfunction, and SNpc DA neuron hyperactivity. Furthermore, the identification of ErbB4/ErbB2 and mGluR1 dysfunction in the FXS model provides novel insights into the molecular mechanisms that go awry in FXS.

Inhibition of nigral ErbB in vivo normalizes SNpc DA neuron activity and repetitive behaviors in the FXS mouse

ASD-like behavioral alterations, including repetitive compulsive behaviors, have been consistently reported in adult *Fmr1* KO mice,

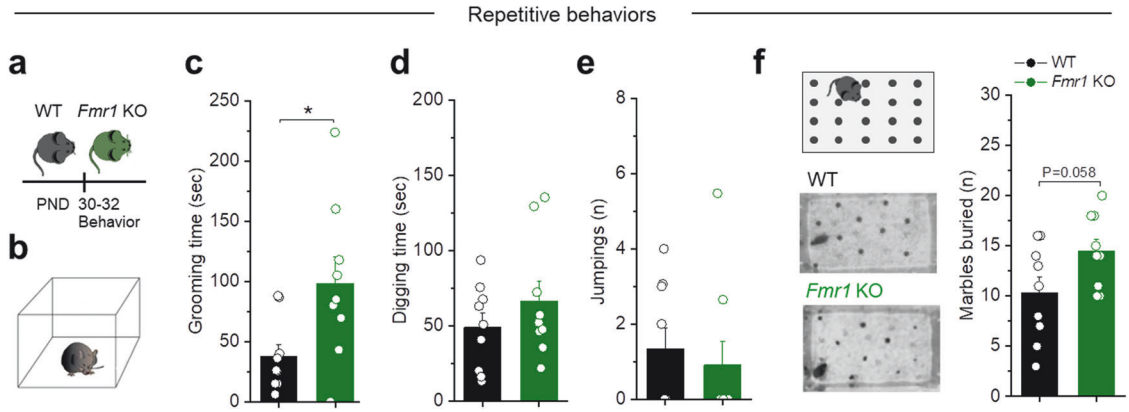

Fig. 4 Early appearance of abnormal repetitive behaviors in adolescent 30-day-old *Fmr1* KO mice. a Timeline of behavioral experiments. **b** Setting for analyses of spontaneous repetitive behaviors and quantifications of time spent in self-grooming (**c**) or digging (**d**), and jumping number (**e**) by *Fmr1* KO (n = 9) and WT (n = 9) mice. Adolescent *Fmr1* KO mice exhibit a selective exacerbation of self-grooming ($p = 0.038$, Mann–Whitney test). Digging time: $p = 0.302$, two-tailed unpaired t test. Jumping (n): $p = 0.612$, Mann–Whitney test). **f** Left, Schematic of marble burying test and example images of tasks executed by WT and *Fmr1* KO mice; Right, Quantification of marbles buried showing increased compulsive burying in the FXS mouse (n = 9 mice for group, $p = 0.058$, two-tailed unpaired t test). All data are presented as mean ± SEM.

with minor variances based on genetic background [54–60]. Differently, adolescent *Fmr1* KO mice have been rarely examined, therefore there is still an inadequate understanding of early behavioral alterations, which better reflect pediatric symptoms of FXS. To advance this knowledge, we evaluated whether adolescent 30-day-old *Fmr1* KO mice displayed abnormal repetitive behaviors (Fig. 4a, b). We observed a selective exacerbation of self-grooming (Fig. 4c), and normal digging (Fig. 4d) and jumping behavior (Fig. 4e) in the FXS mouse. Furthermore, in the marble burying test (also estimating repetitive behaviors) adolescent *Fmr1* KO mice reached higher scores than WT (Fig. 4f). These findings demonstrate early appearance of abnormal repetitive behaviors in the FXS model.

Then, we predicted that abnormal ErbB signaling, by shaping nigral DA neurons activity, would drive compulsive repetitive behaviors in the FXS model. Consistent with this, in vivo inhibition of nigral ErbB signaling should simultaneously rescue nigral DA neuron hyperactivity and repetitive behaviors in the FXS mouse. To assess this hypothesis we first evaluated the effects of in vivo nigral ErbB inhibition on SNpc DA neuron dysfunctions. *Fmr1* KO and WT mice were subjected to cannulation to perform bilateral intra-SNpc injections of PD158780 (10 µM, 0.6 µL) or its vehicle (Veh,0.1% DMSO), followed by patch clamp recordings of nigral DA neurons in midbrain slices of the injected mice (Fig. 5a). We found that nigral ErbB inhibition lowers I_{DHPG} (Fig. 5b) and corrects spontaneous firing hyperactivity (Fig. 5c) and hyperexcitability (Fig. 5d) of SNpc DA neurons of the FXS mouse. Thus, in vivo intra-SNpc ErbB inhibition, by offsetting mGluR1 hyperfunction, normalizes the activity of nigral DA neurons in the FXS model.

To estimate the duration of rescue effects induced by nigral ErbB inhibition, we examined the reemergence of SNpc DA neuron dysfunctions in the FXS mouse after intra-SNpc injection of PD158780 (Fig. 5e). SNpc DA neuron dysfunctions are completely neutralized for at least 4.5 h after intra-SNpc injection of the ErbB inhibitor; after that, at 4.5–6 h after injection, there is partial regain of I_{DHPG} (Fig. 5f) and a trend toward nigral DA neuron hyperactivity (Fig. 5g) and hyperexcitability (Fig. 5h).

To evaluate the effects of the inhibition of nigral ErbB on repetitive behaviors, we examined self-grooming and marble burying behavior in mice subjected to bilateral infusion of the ErbB inhibitor or its vehicle in the SNpc (Fig. 5i). We found that nigral ErbB inhibition rescues exacerbated self-grooming (Fig. 5l) and improves marbles burying behavior of *Fmr1* KO mice (Fig. 5m). General locomotor activity of *Fmr1* KO mice in an open field was not affected (supplementary Fig. S4). This evidence indicates specific reduction of repetitive behaviors of the FXS mouse. Collectively, our findings demonstrate that ErbB inhibition in the SNpc concomitantly rescues dysfunctions of nigral DA neurons and aberrant repetitive behaviors in the FXS model.

Systemic ErbB inhibition corrects SNpc DA neuron dysfunctions and repetitive behaviors of the FXS mouse

To understand if ErbB targeting is a feasible approach for FXS treatment, we examined whether the systemic administration of the ErbB inhibitor is equally effective as intra-SNpc ErbB inhibition in rescuing SNpc DA neuron hyperactivity and repetitive behaviors of the FXS model. Adolescent *Fmr1* KO and WT mice were injected intraperitoneally with PD158780 (10 mg/Kg) or its vehicle (30% DMSO in 0.9% NaCl) and then were subjected to procedures for electrophysiological or behavioral studies (Fig. 6a). First, we performed patch clamp recordings of SNpc DA neurons in midbrain slices from vehicle- or PD158780-treated mice and found that systemic ErbB inhibition mimics the effects of nigral ErbB inhibition, rescuing SNpc DA neuron dysfunctions in the FXS model. Precisely, PD158780-treated *Fmr1* KO mice showed reduced I_{DHPG} (Fig. 6b) and normal spontaneous firing frequency (Fig. 6c) and excitability (Fig. 6d), demonstrating the efficacy of systemic ErbB inhibition in compensating for nigral DA neuron hyperactivity.

In parallel, we analyzed the effects of systemic inhibition of ErbB signaling on abnormal repetitive behaviors of the FXS mouse (Fig. 6e). We found that systemic administration of the ErbB inhibitor rectifies compulsive self-grooming (Fig. 6f) and marble burying behavior of adolescent *Fmr1* KO mice (Fig. 6g), without affecting their general locomotor activity (supplementary Fig. S5). Thus, systemic ErbB inhibition recapitulates rescue effects reliant on inhibition of ErbB in the SNpc. Altogether, these findings demonstrate that systemic administration of the ErbB inhibitor restores normal SNpc DA neuron activity and regular behaviors in the FXS model.

In conclusion, the present manuscript outlines a previously unrealized mechanism contributing to FXS (Fig. 6h). In the FXS model, loss of FMRP in nigral DA neurons drives up-regulation of ErbB4 and ErbB2, subsequently promoting mGluR1 overproduction; in turn, exacerbated ErbB/mGluR1 function enhances firing activity of SNpc DA neurons, fostering the emergence of repetitive behaviors. Consistently, ErbB inhibition in the FXS mouse, by mitigating abnormal mGluR1 tone, neutralizes nigral DA neuron hyperactivity and repetitive behaviors. Collectively, our evidence

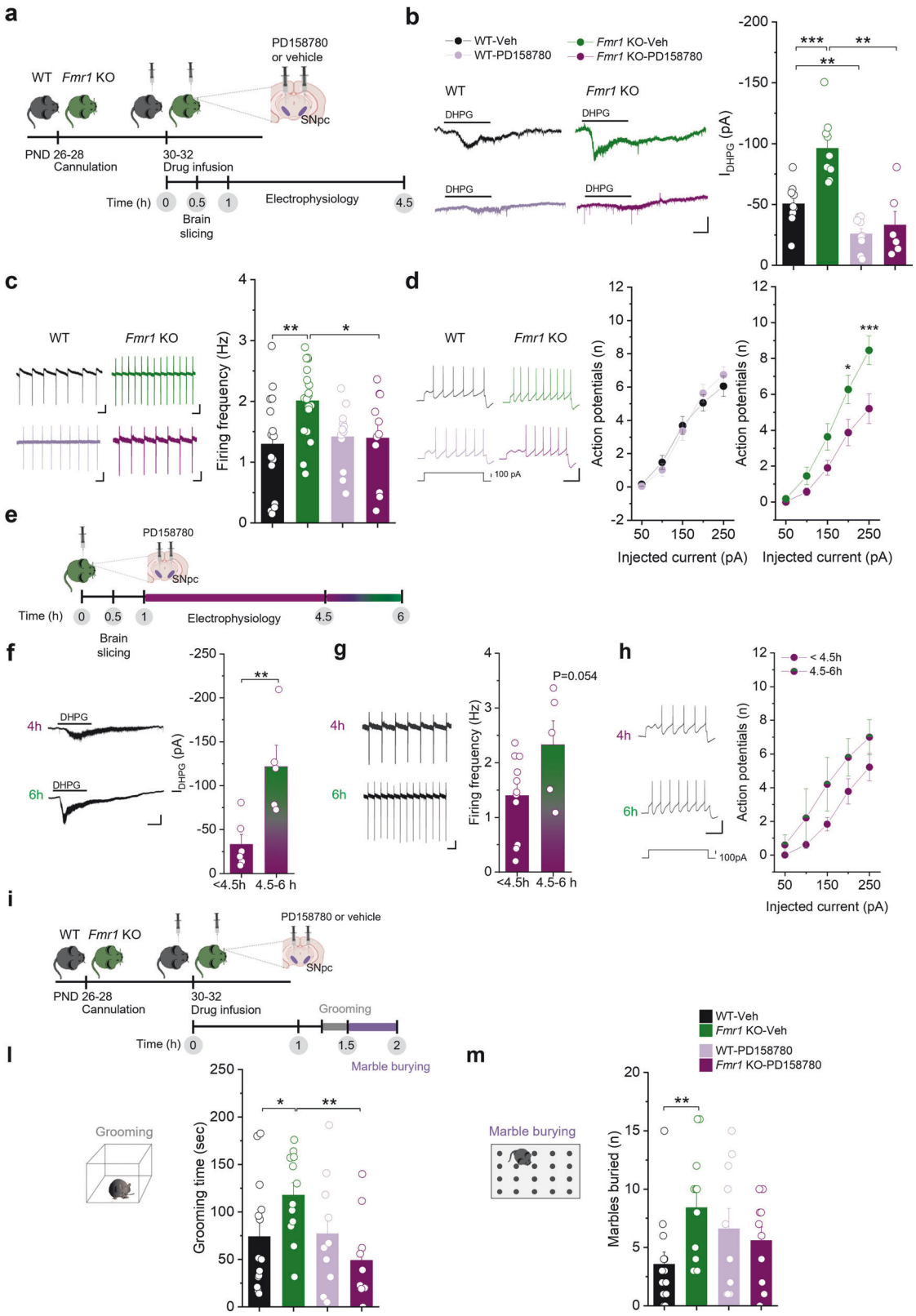

demonstrates that SNpc DA neuron hyperactivity is an early signature of FXS, nigral ErbB4/ErbB2 and mGluR1 play a relevant role in the etiology of FXS, and targeting ErbB represents a valuable pharmacological approach to treat core symptoms of ASD and FXS.

DISCUSSION

Beyond cognitive disability, FXS is characterized by a complex symptomatology, including epilepsy, auditory hypersensitivity, locomotor hyperactivity, anxiety, social avoidance, and repetitive stereotyped behaviors, with a high incidence of autism, diagnosed

Fig. 5 Inhibition of nigral ErbB in vivo normalizes SNpc DA neuron function and reduces abnormal repetitive behaviors in the FXS mouse. a Experimental design to evaluate the effects of nigral ErbB inhibition on SNpc DA neuron dysfunctions in the FXS model. Adolescent mice were subjected to intra-SNpc injections of PD158780 (10 μM) or its vehicle (0.1% DMSO in aCSF) before ex vivo electrophysiology. **b** Example I_{DHPG} traces (left) and plot of I_{DHPG} amplitude (right) showing local ErbB inhibition reduces I_{DHPG} in both genotypes. WT-Vehicle (n = 9 cells/3 mice), WT-PD158780 (n = 9 cells/3 mice), *Fmr1* KO-Vehicle (n = 9 cells/3 mice), and *Fmr1* KO-PD158780 (n = 6 cells/3 mice). Kruskall-Wallis ANOVA followed by Mann–Whitney test. $p = 1.234 \times 10^{-4}$ for ANOVA; $p = 2.879 \times 10^{-4}$ for WT-Vehicle vs *Fmr1* KO-Vehicle, $p = 0.003$ for WT-Vehicle vs WT-PD158780, $p = 0.003$ for *Fmr1* KO-Vehicle vs *Fmr1* KO-PD158780. Scale bar: 50 pA/1 min. **c** Example firing traces (left) and plot of firing frequency (right) proving that nigral ErbB inhibition decreases SNpc DA neuron hyperactivity of the FXS mouse. WT-Vehicle (n = 15 cells/3 mice), WT-PD158780 (n = 12 cells/3 mice), *Fmr1* KO-Vehicle (n = 20 cells/3 mice), and *Fmr1* KO-PD158780 (n = 11 cells/3 mice). Two-way ANOVA followed by Fisher's test. ANOVA: Genotype $p = 0.059$, Drug $p = 0.179$, Genotype X Drug $p = 0.048$. $p = 0.002$ for WT-Vehicle vs *Fmr1* KO-Vehicle, $p = 0.018$ for WT-PD158780 vs *Fmr1* KO-Vehicle, $p = 0.018$ for *Fmr1* KO-Vehicle vs *Fmr1* KO-PD158780. Scale bar: 20pA/0.5 s. **d** Representative evoked APs traces (left) and APs number (right) showing ErbB inhibition offsets hyperexcitability of SNpc DA neurons in the FXS model. WT-Vehicle (n = 19 cells/3 mice) and WT-PD158780 (n = 19 cells/3 mice), RM two-way ANOVA. Drug X Current $p = 0.440$. *Fmr1* KO-Vehicle (n = 22 cells/3 mice) and *Fmr1* KO-PD158780 (n = 18 cells/3 mice), RM two-way ANOVA followed by Tukey's test. ANOVA: Drug $p = 0.073$, Drug X Current $p = 0.015$. $p = 0.018$ at 200 pA, $p = 5.41 \times 10^{-4}$ at 250 pA. Scale bar: 20 mV/0.5 s. **e** Timeline of experiments to analyze the kinetics of ErbB inhibition-induced effects in the FXS mouse. **f** Example I_{DHPG} traces (left) and plot of I_{DHPG} amplitude (right) showing initial rescues of mGluR1 function at 4.5–6 h after intra-SNpc PD158780 injection. I_{DHPG} < 4.5 h (n = 6 cells/3 mice) and I_{DHPG} at 4.5–6 h (n = 5 cells/3 mice); $p = 0.007$, two-tailed unpaired t test. Scale bar: 50 pA/1 min. **g** Representative firing traces (left) and plot of firing frequency (right) of SNpc DA neurons recorded at <4.5 h (n = 11 cells/3 mice) or 4.5–6 h (n = 5 cells/3 mice) after nigral ErbB inhibition. A trend toward hyperactivity is overt at 4.5–6 h after PD158780 injection. $p = 0.054$, two-tailed unpaired t test. Scale bar: 20 pA/0.5 s. **h** Evoked APs traces (left) and APs number (right) showing a trend, still not significant, toward neuronal hyperexcitability in the FXS mouse at 4.5–6 h after PD158780 injection. Post-injection time: <4.5 h (n = 18 cells/3 mice) and 4.5–6 h (n = 5 cells/3 mice). RM two-way ANOVA. Time $p = 0.202$, Time X Current $p = 0.865$. Scale bar: 20 pA/0.5 s. All data are presented as mean ± SEM. **i** Experimental design to evaluate the effects of ErbB inhibition in the SNpc on repetitive behaviors of adolescent mice. **l** Plot of time spent in self-grooming showing that nigral ErbB inhibition rescues this repetitive behavior in the FXS mouse. WT-Vehicle (n = 14), WT-PD158780 (n = 10), *Fmr1* KO-Vehicle (n = 12), and *Fmr1* KO-PD158780 (n = 10). Two-way ANOVA followed by Fisher's test. ANOVA: Drug $p = 0.041$, Genotype X Drug $p = 0.026$. $p = 0.040$ for WT-Vehicle vs *Fmr1* KO-Vehicle; $p = 0.003$ for *Fmr1* KO-Vehicle vs *Fmr1* KO-PD158780. **m** Number of marbles buried indicating that nigral ErbB inhibition attenuates marble burying in the FXS model. WT-Vehicle (n = 14), WT-PD158780 (n = 10), *Fmr1* KO-Vehicle (n = 12), and *Fmr1* KO-PD158780 (n = 10). Two-way ANOVA followed by Fisher's test. ANOVA: Genotype X Drug $p = 0.033$. $p = 0.008$ for WT-vehicle vs *Fmr1* KO-vehicle, $p = 0.147$ for *Fmr1* KO-vehicle vs *Fmr1* KO-PD158780.

in approximately 50% of males and 20% of females with FXS [2, 61, 62]. Multifaceted symptomatology advises the contribution of multiple brain areas; indeed, functional alterations have been described in the hippocampus, cortex, thalamus, cerebellum, amygdala, and striatum of FXS models and patients [3, 34, 62]. Although the SNpc DA nucleus is a central hub for movement control and the creation of habits and sequential behaviors, and could be expected that its dysfunction triggers compulsive and stereotyped behaviors [14, 15], research aimed at identifying dysfunctions of nigral DA neurons in ASD and FSX models has been neglected so far. Here, we provide the first direct evidence of early dysregulation of the SNpc DA nucleus in FXS, revealing various functional changes that occur in nigral DA neurons of the FXS mouse in adolescence since the third postnatal week. Precisely, SNpc DA neurons in the FXS mouse display increased spontaneous firing rate and hyperexcitability, in addition to alterations in passive membrane properties, namely increased C_m. Since C_m depends on membrane size and composition, higher C_m may reflect hypertrophic changes in the soma or dendritic arbor and/or altered lipidic double-bilayer composition or thickness. Notably, increased density of TH+ fibers in the striatum of 3-month-old *Fmr1* KO has been recently described, suggesting hypertrophic changes in nigral DA neurons in adulthood [20].

Neuronal hyperexcitability is a recurrent signature in FXS, associated with abnormal circuit connectivity in different brain areas, including the somatosensory and entorhinal cortex, auditory brainstem, and hippocampus [34]. Diverse and apparently area-specific underlying mechanisms have been identified, including E/I imbalance (i.e., increased glutamatergic or reduced GABAergic transmission), or dysfunctions in different types of K^+ and Na^+ channels, such as voltage-dependent Kv3.1 or Ca^{2+}-activated K^+ channels (SK and BK) or Na^+ channels (Slack, and those carrying persistent or transient Na^+ currents, I_{NaP} and I_{NaT}) [34, 63–69]. Ion channels alterations can directly arise from increased translation or loss of physical FMRP-channels interaction; otherwise, they can be secondary to abnormal expression/activity of upstream regulators, as reported for mGluR5 [66, 70]. The present manuscript advances the understanding of FXS substrates by revealing that mGluR1 hyperfunction drives nigral DA neuron hyperactivity and hyperexcitability in the FXS model. In addition to directly evidencing higher mGluR1-induced currents (I_{DHPG} in MPEP), we show that mGluR1 inhibition normalizes the spontaneous firing rate and excitability of SNpc DA neurons in the FXS mouse.

Knowledge about mGluR1 role in FXS etiology is rather limited: some evidence indicates that systemic mGluR1 inhibition ameliorates behavioral phenotypes such as audiogenic seizures, hyperlocomotion, and marble burying in adult *Fmr1* KO mice [71, 72], but precise information on brain areas, cellular loci, and specific mGluR1-dependent mechanism contributing to FXS is lacking. Contrariwise, mGluR5 has been in the spotlight of intense investigations in the FXS field since decades: exacerbated mGluR5 function is considered an FXS hallmark and motivated the "mGluR theory of FXS" [73], which assumes that mGluR5 hyperfunction determines synaptic, behavioral, and cognitive FXS alterations. However, while mGluR5 inhibition attenuates some FXS phenotypes in preclinical models [74–76], mGluR5-based therapeutics returned with limited efficacy in human clinical trials [77], exposing the need to identify additional targets or collateral mechanisms beyond mGluR5 hyperfunction. Our data support the implication of mGluR1 in FXS etiology, proving its key role in influencing nigrostriatal DA circuit. Interestingly, a recent study attested *Grm1* association (encoding for mGluR1) with schizophrenia [78]; thus, mGluR1 dysfunction seems to be a shared feature of schizophrenia and FXS.

Different mechanisms could underlie mGluR1 hyperfunction in nigral DA neurons of the FXS model, that is, 1) increased glutamate release, acting on the same mGluR1 pool, 2) enhanced mGluR1 levels in the membrane, with or without variation in ambient glutamate, or 3) abnormal mGluR1 constitutive activity (ligand-independent signaling) associated or not with changes in its levels. Analyses of glutamatergic synaptic inputs to nigral DA neurons exclude that increased glutamate release promotes mGluR1 hyperfunction and nigral DA neuron hyperactivity. In addition, normal GABAergic synaptic inputs similarly indicate that neuronal hyperactivity is not reliant on synaptic disinhibition. Diversely, we found higher mGluR1 levels in total protein extracts

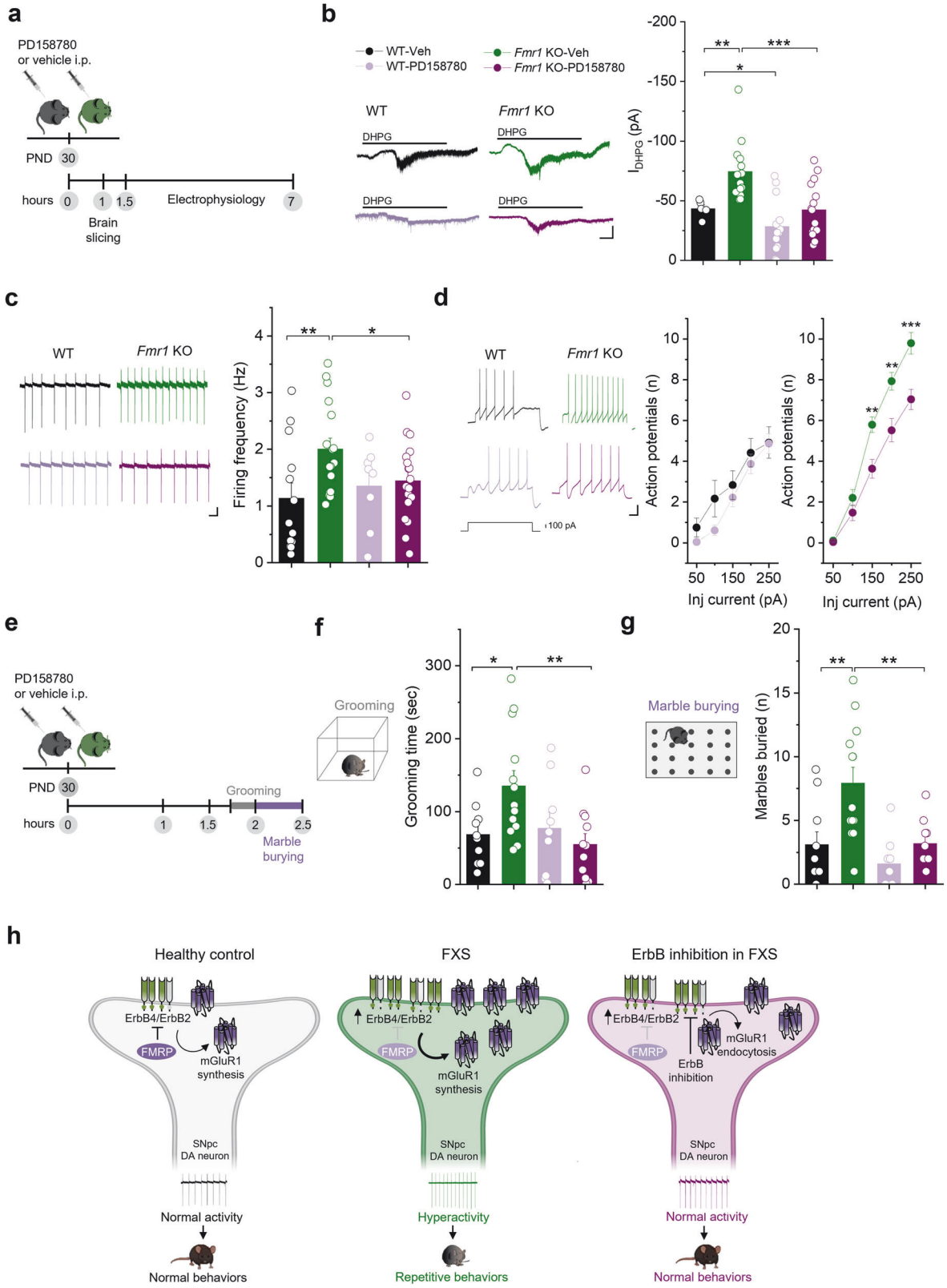

from SNpc homogenates and increased mGluR1 optical density in SNpc TH+ neurons of adolescent FXS mice, which demonstrate mGluR1 up-regulation within SNpc DA neurons. This figures out as a nigral DA neuron-specific mechanism, as mGluR1 overexpression is not overt in the VTA of *Fmr1* KO mice. Therefore, an enrichment of the membrane-expressed mGluR1 pool, despite regular glutamate release, maintains mGluR1 hyperfunction and nigral DA neuron hyperactivity in the FXS mouse.

We have previously reported that ErbB signaling controls mGluR1 expression and function within SNpc DA neurons of WT

Fig. 6 Systemic ErbB inhibition corrects SNpc DA neuron dysfunctions and repetitive behaviors of the FXS mouse. a Experimental design to evaluate the effects of systemic ErbB inhibition on SNpc DA neuron functions. **b** Example I_{DHPG} traces (left) and quantification of I_{DHPG} amplitude (right) in WT-Vehicle (n = 5 cells/2 mice), WT-PD158780 (n = 13 cells/3 mice), *Fmr1* KO-Vehicle (n = 14 cells/3 mice), and *Fmr1* KO-PD158780 (n = 15 cells/3 mice). Kruskal-Wallis ANOVA followed by Kolmogorov-Smirnov test. ANOVA: $p = 0.001$. $p = 0.039$ for WT-Vehicle vs WT-PD158780, $p = 0.001$ for WT-Vehicle vs *Fmr1* KO-Vehicle, $p = 8.123 \times 10^{-4}$ for *Fmr1* KO-Vehicle vs *Fmr1* KO-PD158780. Scale bar: 50 pA/0.5 s. **c** Example spontaneous firing traces (left) and firing frequency plot (right) of WT-Vehicle (n = 13 cells/2 mice), WT-PD158780 (n = 8 cells/3 mice), *Fmr1* KO-Vehicle (n = 17 cells/3 mice), and *Fmr1* KO-PD158780 (n = 18 cells/3 mice). Two-way ANOVA followed by Fisher's test. ANOVA: Genotype $p = 0.038$, Genotype X Drug $p = 0.093$. $p = 0.005$ for WT-Vehicle vs *Fmr1* KO-Vehicle, $p = 0.045$ *Fmr1* KO-Vehicle vs *Fmr1* KO-PD158780. Scale bar: 10 pA/0.5 s. **d** Evoked APs traces (left) and APs number plot (right). Effects in WT mice: WT-Vehicle (n = 12 cells/2 mice) and WT-PD158780 (n = 23 cells/3 mice). RM two-way ANOVA. Drug $p = 0.393$, Drug X Current $p = 0.768$. Effect in *Fmr1* KO mice: *Fmr1* KO-Vehicle (n = 29 cells/3 mice) and *Fmr1* KO-PD158780 (n = 25 cells/3 mice). RM two-way ANOVA followed by Bonferroni test. ANOVA: Drug $p = 1.76 \times 10^{-4}$, Drug X Current $p = 2.699 \times 10^{-4}$. $p = 0.009$ at 150 pA, $p = 0.003$ at 200 pA, $p = 3.003 \times 10^{-4}$. Scale bar: 20 mV/0.5. **e** Experimental protocol to analyze the effects of systemic ErbB inhibition on aberrant repetitive behaviors in adolescent FXS mice. **f** Plot of time spent in self-grooming by WT-Vehicle (n = 10), WT-PD158780 (n = 9), *Fmr1* KO-Vehicle (n = 13), and *Fmr1* KO-PD158780 (n = 11). Two-way ANOVA followed by Fisher's test. ANOVA: Genotype X Drug $p = 0.023$. $p = 0.012$ for WT-Vehicle vs *Fmr1* KO-Vehicle, $p = 0.002$ for *Fmr1* KO-PD158780 vs *Fmr1* KO-Vehicle. **g** Number of marbles buried by WT-Vehicle (n = 10), WT-PD158780 (n = 9), *Fmr1* KO-Vehicle (n = 13) and *Fmr1* KO-PD158780 (n = 11). Two-way ANOVA followed by Bonferroni test. ANOVA: Genotype $p = 0.001$, Drug $p = 0.002$, Genotype X Drug $p = 0.099$. $p = 0.004$ for WT-Vehicle vs *Fmr1* KO-Vehicle, $p = 0.004$ for *Fmr1* KO-Vehicle vs *Fmr1* KO-PD158780. **h** Cartoon of molecular mechanisms underlying SNpc DA neuron hyperactivity and repetitive behaviors in the FXS model and the rescues effects induced by ErbB inhibition. Left) In the healthy brain, ErbB4/ErbB2 signaling fine-tunes mGluR1 expression and function in nigral DA neurons, contributing to keep firing activity at physiological levels instrumental to normal behaviors. Middle) In the FXS model, FMRP deficiency induces ErbB4 and ErbB2 up-regulation and consequential mGluR1 overproduction in nigral DA neurons. This exacerbated ErbB/mGluR1 function induces neuronal hyperactivity and hyperexcitability, leading to abnormal activation of nigrostriatal DA circuit and insurgence of repetitive behaviors. Right) ErbB inhibition in the FXS model, by triggering mGluR1 endocytosis, neutralizes aberrant ErbB/mGluR1-dependent effects within nigral DA neurons, restoring normal firing activity and regular behaviors.

rodents [27, 35, 40, 79]. Precisely, NRG-activated ErbB signaling induces de novo synthesis and trafficking of mGluR1 to membranes, potentiating mGluR1-dependent effects, such as I_{DHPG}, but also long-term depression [27, 40]. Contrariwise, ErbB inhibition stimulates mGluR1 endocytosis in SNpc DA neurons, promptly disrupting all mGluR1 functions [27, 35, 40, 79]. In light of this functional liaison between ErbB and mGluR1, and since ErbB4 and ErbB2 are putative FMRP targets [50–53], we hypothesized that ErbB4/ErbB2 up-regulation may cause abnormal de novo synthesis of mGluR1 inside nigral DA neurons. Coherently, ErbB4 and ErbB2 levels, besides mGluR1, are increased in SNpc DA neurons, and with up-regulation gradients (ErbB4 and ErbB2 > mGluR1) supporting a hierarchic relationship. This supports an amplification of ErbB-induced mGluR1 synthesis [27] in the FXS model.

NRGs/ErbB signaling is essential for correct neurodevelopment, by affecting neuronal migration, axon guidance, glia differentiation, myelination, neurite outgrowth, and synapses formation [80], as well as for adult brain functions, by shaping synaptic transmission and plasticity [79]. NRGs/ErbB dysregulation has recently been advanced in ASD, based on evidence of *Nrg1* polymorphisms [45, 46] and altered NRGs levels in blood from idiopathic ASD patients [47–49]; however, clinical studies reported divergent modifications, thus requiring further investigations. Preclinical analyses of NRGs/ErbB pathway in ASD models is scarce, being limited to a report showing increased NRGs levels (NRG3 and NRG1 type II) in microglia of BTBR mice (an idiopathic ASD model) [47], and a study on ErbB inhibition-induced effects on hippocampal synaptic plasticity and contextual fear memory in a model of Angelman syndrome [81]. Due to this restricted evidence, the factual contribution of NRGs/ErbB signaling in ASD remains elusive. Remarkably, despite its key role in neurodevelopment, NRGs/ErbB signaling has not been previously evaluated in FXS. Thus, our evidence of up-regulation of ErbB4 and ErbB2 in nigral DA neurons of the FXS mouse represents the first demonstration of NRGs/ErbB dysregulation in FXS. Notably, NRG1 expression in SNpc is regular in adolescent *Fmr1* KO mice. While ErbB4/ErbB2 up-regulation per se can sustain enhanced ErbB signaling, despite normal amounts of ligands, we do not exclude that other NRGs subtypes beyond NRG1 could be up-regulated and future investigations might reveal these variations. Regardless of the precise ligand, our data prove that ErbB4/ErbB2 up-regulation during critical developmental stages alters nigrostriatal DA circuit activity; counteracting nigral ErbB signaling, by in situ injection of an ErbB4 and ErbB2 inhibitor, besides blunting mGluR1-activated currents, normalizes spontaneous firing rate and excitability of SNpc DA neurons. Thus, tuning down ErbB signaling in the FXS mouse rescues nigral DA neuron functions.

We have previously reported that in vivo activation of nigral mGluR1 increases striatal DA release in rats, and this can be prevented by inhibiting ErbB [27]. Based on this and previous indications that striatal DA tone affects repetitive behaviors in wild-type rodents, we predicted that ErbB/mGluR1-dependent nigral DA neuron hyperactivity, by affecting striatal DA levels, triggers repetitive behaviors in the FXS model. Soundly with this idea, exacerbated repetitive behaviors (self-grooming and marble burying) are overt in the FXS mouse at 30 days of age, a time-point at which nigral DA neurons hyperactivity is well-established. Importantly, these data describe the earliest appearance of ASD-like repetitive behaviors in *Fmr1* KO mice, previously reported in older animals (>7 weeks) [56, 58, 60, 82].

According to our prediction, in vivo nigral ErbB inhibition concomitantly rescues SNpc DA neuron functions (by decreasing I_{DHPG} and normalizing spontaneous firing rate and excitability) and repetitive behaviors (by reducing self-grooming and marble burying). This proves a causal role for abnormal ErbB signaling, by activating the SNpc DA nucleus, in triggering repetitive behaviors in the FXS mouse. Consistent with this concept that ErbB overstimulation in early developmental stages promotes nigral DA neuron hyperactivity, subchronic neonatal exposure to NRG1 in wild-type mice (P2-10) increases SNpc DA neuron activity in adulthood [83].

Importantly, systemic administration of the ErbB inhibitor in the FXS mouse mimics the rescue effects induced by nigral ErbB inhibition, by rectifying concurrently SNpc DA neuron dysfunctions and repetitive behaviors. Thus, besides revealing a novel mechanism - ErbB/mGluR1-dependent SNpc DA neuron hyperactivity - instrumental to repetitive behaviors, we demonstrate that ErbB inhibition, also via a practicable route of administration, effectively reduces FXS symptoms.

Furthermore, we provide insights on the duration of ErbB inhibition, as this is key information to design valid pharmacological protocols in the perspective of a clinical application. The kinetics of reemergence of the former dysfunctions in SNpc DA

neurons of the FXS mouse indicates maintenance of the ErbB-induced effects for at least 4.5 h after intranigral drug injection and 7 h after systemic administration. Thus, a single treatment with the ErbB inhibitor produces lasting correction of the SNpc DA neuron dysfunctions underlying repetitive behaviors.

To date, there are no FDA-approved compounds for the treatment of repetitive behaviors in ASD and FXS patients. Current pharmacotherapy stands on off-label use of antipsychotics, which despite some positive effects, display adverse effects that undermine their therapeutic benefit [84]. Therefore, identifying novel therapeutic approaches to offset processes instrumental in repetitive behaviors remains an important mission. Besides gaining insight into the mechanisms that go awry in FXS, the present study demonstrate that targeting ErbB is an effective therapeutic strategy for aberrant repetitive behaviors. Beyond ASD and FXS, repetitive compulsive behaviors are hallmarks of different neuropsychiatric diseases, including obsessive-compulsive disorder and Tourette syndrome: rodent self-grooming is considered a translating phenotype of excoriation (compulsive skin picking), trichotillomania (compulsive hair pulling), dysmorphic disorder (obsessive cosmetic grooming) and tics, key features of these human diseases [85, 86]. In this view, ErbB inhibition could be beneficial for the treatment of repetitive behaviors in different neuropsychiatric and neurodevelopmental diseases, in addition to ASD and FXS. Importantly, the therapeutic effectiveness also via systemic administration certifies the factual practicality of the ErbB inhibition-based approach, laying solid bases to propose ErbB targeting in clinical evaluations in ASD and FXS patients.

DATA AVAILABILITY

Source data generated in the current study are available from the corresponding author on reasonable request. Supplementary information is available at MP's website.

REFERENCES

1. Leekam SR, Prior MR, Uljarevic M. Restricted and repetitive behaviors in autism spectrum disorders: a review of research in the last decade. Psychol Bull. 2011;137:562–93.
2. Oakes A, Thurman AJ, McDuffie A, Bullard LM, Hagerman RJ, Abbeduto L. Characterising repetitive behaviours in young boys with fragile X syndrome. J Intellect Disabil Res. 2016;60:54–67.
3. Bagni C, Zukin RS. A synaptic perspective of fragile X syndrome and autism spectrum disorders. Neuron. 2019;101:1070–88.
4. Redgrave P, Rodriguez M, Smith Y, Rodriguez-Oroz MC, Lehericy S, Bergman H, et al. Nat Rev Neurosci. 2010;11:760–72.
5. Howard CD, Li H, Geddes CE, Jin X. Dynamic nigrostriatal dopamine biases action selection. Neuron. 2017;93:1436–1450e1438.
6. Ernst AM, Smelik PG. Site of action of dopamine and apomorphine on compulsive gnawing behavior in rats. Experientia. 1966;22:837–8.
7. Canales JJ, Graybiel AM. A measure of striatal function predicts motor stereotypy. Nat Neurosci. 2000;3:377–83.
8. Berridge KC, Aldridge JW. Super-stereotypy II: enhancement of a complex movement sequence by intraventricular dopamine D1 agonists. Synapse. 2000;37:205–15.
9. Presti MF, Mikes HM, Lewis MH. Selective blockade of spontaneous motor stereotypy via intrastriatal pharmacological manipulation. Pharmacol Biochem Behav. 2003;74:833–9.
10. Berridge KC, Aldridge JW, Houchard KR, Zhuang X. Sequential super-stereotypy of an instinctive fixed action pattern in hyper-dopaminergic mutant mice: a model of obsessive compulsive disorder and Tourette's. BMC Biol. 2005;3:4.
11. Cromwell HC, Berridge KC, Drago J, Levine MS. Action sequencing is impaired in D1A-deficient mutant mice. Eur J Neurosci. 1998;10:2426–32.
12. Lee Y, Kim H, Kim J, Park J, Choi J, Lee J, et al. Excessive D1 dopamine receptor activation in the dorsal striatum promotes autistic-like behaviors. Mol Neurobiol. 2018;55:5658–71.
13. Xue J, Qian D, Zhang B, Yang J, Li W, Bao Y, et al. Midbrain dopamine neurons arbiter OCD-like behavior. Proc Natl Acad Sci USA. 2022;119:e2207545119.
14. Pavăl DA. Dopamine hypothesis of autism spectrum disorder. Dev Neurosci. 2017;39:355–60.
15. Pavăl D, Micluția IV. The dopamine hypothesis of autism spectrum disorder revisited: current status and future prospects. Dev Neurosci. 2021;43:73–83.
16. Gandhi T, Lee CC. Neural mechanisms underlying repetitive behaviors in rodent models of autism spectrum disorders. Front Cell Neurosci. 2021;14:592710.
17. Kosillo P, Bateup HS. Dopaminergic dysregulation in syndromic autism spectrum disorders: insights from genetic mouse models. Front Neural Circuits. 2021;15:700968.
18. Longo F, Aryal S, Anastasiades PG, Maltese M, Baimel C, Albanese F, et al. Cell-type-specific disruption of cortico-striatal circuitry drives repetitive patterns of behavior in fragile X syndrome model mice. Cell Rep. 2023;42:112901.
19. Mercaldo V, Vidimova B, Gastaldo D, Fernández E, Lo AC, Cencelli G, et al. Altered striatal actin dynamics drives behavioral inflexibility in a mouse model of fragile X syndrome. Neuron. 2023;111:1760–75.
20. Chao OY, Pathak SS, Zhang H, Dunaway N, Li JS, Mattern C, et al. Altered dopaminergic pathways and therapeutic effects of intranasal dopamine in two distinct mouse models of autism. Mol Brain. 2020;13:111.
21. Fish EW, Krouse MC, Stringfield SJ, Diberto JF, Robinson JE, Malanga CJ. Changes in sensitivity of reward and motor behavior to dopaminergic, glutamatergic, and cholinergic drugs in a mouse model of fragile X syndrome. PLoS One. 2013;8:e77896.
22. Gruss M, Braun K. Alterations of amino acids and monoamine metabolism in male *Fmr1* knockout mice: a putative animal model of the human fragile X mental retardation syndrome. Neural Plast. 2001;8:285–98.
23. Sørensen EM, Bertelsen F, Weikop P, Skovborg MM, Banke T, Drasbek KR, et al. Hyperactivity and lack of social discrimination in the adolescent *Fmr1* knockout mouse. Behav Pharmacol. 2015;26:733–40.
24. Ventura R, Pascucci T, Catania MV, Musumeci SA, Puglisi-Allegra S. Object recognition impairment in *Fmr1* knockout mice is reversed by amphetamine: involvement of dopamine in the medial prefrontal cortex. Behav Pharmacol. 2004;15:433–42.
25. Fulks JL, O'bryhim BE, Wenzel SK, Fowler SC, Vorontsova E, Pinkston JW, et al. Dopamine release and uptake impairments and behavioral alterations observed in mice that model fragile X mental retardation syndrome. ACS Chem. Neurosci. 2010;1:679–90.
26. Paxinos G, Franklin KBJ. The mouse brain in stereotaxic coordinates. 5th Edition - Hardback ISBN: 9780128161579 (2019).
27. Ledonne A, Nobili A, Latagliata EC, Cavallucci V, Guatteo E, Puglisi-Allegra S, et al. Neuregulin 1 signalling modulates mGluR1 function in mesencephalic dopaminergic neurons. Mol Psychiatry. 2015;20:959–73.
28. Ledonne A, Mango D, Latagliata EC, Chiacchierini G, Nobili A, Nisticò R, et al. Neuregulin 1/ErbB signalling modulates hippocampal mGluRI-dependent LTD and object recognition memory. Pharmacol Res. 2018;130:12–24.
29. Gu Y, Tran T, Murase S, Borrell A, Kirkwood A, Quinlan EM. Neuregulin-dependent regulation of fast-spiking interneuron excitability controls the timing of the critical period. J Neurosci. 2016;36:10285–95.
30. Price R, Ferrari E, Gardoni F, Mercuri NB, Ledonne A. Protease-activated receptor 1 (PAR1) inhibits synaptic NMDARs in mouse nigral dopaminergic neurons. Pharmacol Res. 2020;160:105185.
31. Ledonne A, Massaro Cenere M, Paldino E, D'Angelo V, D'Addario SL, Casadei N, et al. Morpho-functional changes of nigral dopamine neurons in an α-synuclein model of Parkinson's disease. Mov Disord. 2023;38:256–66.
32. Angoa-Pérez M, Kane MJ, Briggs DI, Francescutti DM, Kuhn DM. Marble burying and nestlet shredding as tests of repetitive, compulsive-like behaviors in mice. J Vis Exp. 2013;24:50978.
33. Gantz SC, Ford CP, Morikawa H, Williams JT. The evolving understanding of dopamine neurons in the substantia nigra and ventral tegmental area. Annu Rev Physiol. 2018;80:219–41.
34. Deng PY, Klyachko VA. Channelopathies in fragile X syndrome. Nat Rev Neurosci. 2021;22:275–89.
35. Ledonne A, Mercuri NB. Insights on the functional interaction between group 1 metabotropic glutamate receptors (mGluRI) and ErbB receptors. Int J Mol Sci. 2020;21:7913.
36. Mango D, Ledonne A. Updates on the physiopathology of group I metabotropic glutamate receptors (mGluRI)-dependent long-term depression. Cells. 2023;12:1588.
37. Mercuri NB, Stratta F, Calabresi P, Bonci A, Bernardi G. Activation of metabotropic glutamate receptors induces an inward current in rat dopamine mesencephalic neurons. Neuroscience. 1993;56:399–407.
38. Guatteo E, Mercuri NB, Bernardi G, Knöpfel T. Group I metabotropic glutamate receptors mediate an inward current in rat substantia nigra dopamine neurons that is independent from calcium mobilization. J Neurophysiol. 1999;82:1974–81.

39. Prisco S, Natoli S, Bernardi G, Mercuri NB. Group I metabotropic glutamate receptors activate burst firing in rat midbrain dopaminergic neurons. Neuropharmacology. 2002;42:289–96.
40. Ledonne A, Mercuri NB. mGluR1-dependent long term depression in rodent midbrain dopamine neurons is regulated by neuregulin 1/ErbB signaling. Front Mol Neurosci. 2018;11:346.
41. Stefansson H, Sigurdsson E, Steinthorsdottir V, Bjornsdottir S, Sigmundsson T, Ghosh S, et al. Neuregulin 1 and susceptibility to schizophrenia. Am J Hum Genet. 2002;71:877–92.
42. Harrison PJ, Law AJ. Neuregulin 1 and schizophrenia: genetics, gene expression, and neurobiology. Biol Psychiatry. 2006;60:132–40.
43. Li D, Collier DA, He L. Meta-analysis shows strong positive association of the neuregulin 1 (NRG1) gene with schizophrenia. Hum Mol Genet. 2006;15:1995–2002.
44. Nicodemus KK, Law AJ, Radulescu E, Luna A, Kolachana B, Vakkalanka R, et al. Biological validation of increased schizophrenia risk with NRG1, ERBB4, and AKT1 epistasis via functional neuroimaging in healthy controls. Arch Gen Psychiatry. 2010;67:991–1001.
45. Yoo HJ, Woo RS, Cho SC, Kim BN, Kim JW, Shin MS, et al. Genetic association analyses of neuregulin 1 gene polymorphism with endopheontype for sociality of Korean autism spectrum disorders family. Psychiatry Res. 2015;227:366–8.
46. Prats C, Fatjó-Vilas M, Penzol MJ, Kebir O, Pina-Camacho L, Demontis D, et al. Association and epistatic analysis of white matter related genes across the continuum schizophrenia and autism spectrum disorders: the joint effect of NRG1-ErbB genes. World J Biol Psychiatry. 2022;23:208–18.
47. Ikawa D, Makinodan M, Iwata K, Ohgidani M, Kato TA, Yamashita Y, et al. Microglia-derived neuregulin expression in psychiatric disorders. Brain Behav Immun. 2017;61:375–85.
48. Esnafoglu E. Levels of peripheral Neuregulin 1 are increased in non-medicated autism spectrum disorder patients. J Clin Neurosci. 2018;57:43–45.
49. Abbasy S, Shahraki F, Haghighatfard A, Qazvini GM, Rafiei ST, Noshadirad E, et al. Neuregulin1 types mRNA level changes in autism spectrum disorder, and is associated with deficit in executive functions. EBioMedicine. 2018;37:483–8.
50. Darnell JC, Van Driesche SJ, Zhang C, Hung KY, Mele A, Fraser CE, et al. FMRP stalls ribosomal translocation on mRNAs linked to synaptic function and autism. Cell. 2011;146:247–61.
51. Ascano, MJr, Mukherjee N, Bandaru P, Miller JB, Nusbaum JD, et al. FMRP targets distinct mRNA sequence elements to regulate protein expression. Nature. 2012;492:382–6.
52. Maurin T, Lebrigand K, Castagnola S, Paquet A, Jarjat M, Popa A, et al. HITS-CLIP in various brain areas reveals new targets and new modalities of RNA binding by fragile X mental retardation protein. Nucleic Acids Res. 2018;46:6344–55.
53. Hale CR, Sawicka K, Mora K, Fak JJ, Kang JJ, Cutrim P, et al. FMRP regulates mRNAs encoding distinct functions in the cell body and dendrites of CA1 pyramidal neurons. Elife. 2021;10:e71892.
54. Bakker C, Verheij C, Willemsen R, Vanderhelm R, Oerlemans F, Vermey M, et al. Fmr1 knockout mice: a model to study fragile X mental retardation. The Dutch-Belgian Fragile X Consortium. Cell. 1994;78:23–33.
55. Mineur YS, Sluyter F, de Wit S, Oostra BA, Crusio WE. Behavioral and neuroanatomical characterization of the Fmr1 knockout mouse. Hippocampus. 2002;12:39–46.
56. Pietropaolo S, Guilleminot A, Martin B, D'Amato F, Crusio W. Genetic-background modulation of core and variable autistic-like symptoms in Fmr1 knock-out mice. PLoS One. 2011;6:e17073.
57. Spencer CM, Alekseyenko O, Hamilton SM, Thomas AM, Serysheva E, Yuva-Paylor LA, et al. Modifying behavioral phenotypes in Fmr1KO mice: genetic background differences reveal autistic-like responses. Autism Res. 2011;4:40–56.
58. Veeraragavan S, Graham D, Bui N, Yuva-Paylor LA, Wess J, Paylor R. Genetic reduction of muscarinic M4 receptor modulates analgesic response and acoustic startle response in a mouse model of fragile X syndrome (FXS). Behav Brain Res. 2012;228:1–8.
59. Dolan BM, Duron SG, Campbell DA, Vollrath B, Rao BSS, Ko H-Y, et al. Rescue of fragile X syndrome phenotypes in Fmr1 KO mice by the small-molecule PAK inhibitor FRAX486. Proc Natl Acad Sci USA. 2013;110:5671–6.
60. Gantois I, Khoutorsky A, Popic J, Aguilar-Valles A, Freemantle E, Cao R, et al. Metformin ameliorates core deficits in a mouse model of fragile X syndrome. Nat Med. 2017;23:674–7.
61. Kaufmann WE, Kidd SA, Andrews HF, Budimirovic DB, Esler A, Haas-Givler B, et al. Autism spectrum disorder in fragile X syndrome: cooccurring conditions and current treatment. Pediatrics. 2017;139:S194–S206.
62. Hagerman RJ, Berry-Kravis E, Hazlett HC, Bailey JrDB, Moine H, Kooy RF, et al. Fragile X syndrome. Nat Rev Dis Primers. 2017;3:17065.
63. Gibson JR, Bartley AF, Hays SA, Huber KM. Imbalance of neocortical excitation and inhibition and altered UP states reflect network hyperexcitability in the mouse model of fragile X syndrome. J Neurophysiol. 2008;100:2615–26.
64. Goncalves JT, Anstey JE, Golshani P, Portera-Cailliau C. Circuit level defects in the developing neocortex of fragile X mice. Nat Neurosci. 2013;16:903–9.
65. Domanski APF, Booker SA, Wyllie DJA, Isaac JTR, Kind PC. Cellular and synaptic phenotypes lead to disrupted information processing in Fmr1-KO mouse layer 4 barrel cortex. Nat Commun. 2019;10:4814.
66. Deng PY, Klyachko VA. Increased persistent sodium current causes neuronal hyperexcitability in the entorhinal cortex of Fmr1 knockout mice. Cell Rep. 2016;16:3157–66.
67. Deng PY, Carlin D, Oh YM, Myrick LK, Warren ST, Cavalli V, et al. Voltage-independent SK-channel dysfunction causes neuronal hyperexcitability in the hippocampus of Fmr1 knock- out mice. J Neurosci. 2019;39:28–43.
68. Routh BN, Rathour RK, Baumgardner ME, Kalmbach BE, Johnston D, Brager DH. Increased transient Na+ conductance and action potential output in layer 2/3 prefrontal cortex neurons of the fmr1–/y mouse. J Physiol. 2017;595:4431–48.
69. El-Hassar L, Song L, Tan WJT, Large CH, Alvaro G, Santos-Sacchi J, et al. Modulators of Kv3 potassium channels rescue the auditory function of fragile X mice. J Neurosci. 2019;39:4797–813.
70. Chuang S-C, Zhao W, Bauchwitz R, Yan Q, Bianchi R, Wong RKS. Prolonged epileptiform discharges induced by altered group I metabotropic glutamate receptor-mediated synaptic responses in hippocampal slices of a fragile X mouse model. Comparative Study J Neurosci. 2005;25:8048–55.
71. Thomas AM, Bui N, Graham D, Perkins JR, Yuva-Paylor LA, Paylor R. Genetic reduction of group 1 metabotropic glutamate receptors alters select behaviors in a mouse model for fragile X syndrome. Behav Brain Res. 2011;223:310–21.
72. Thomas AM, Bui N, Perkins JR, Yuva-Paylor LA, Paylor R. Group I metabotropic glutamate receptor antagonists alter select behaviors in a mouse model for fragile X syndrome. Psychopharmacology (Berl). 2012;219:47–58.
73. Bear MF, Huber KM, Warren ST. The mGluR theory of fragile X mental retardation. Review Trends Neurosci. 2004;27:370–7.
74. Yan QJ, Rammal M, Tranfaglia M, Bauchwitz RP. Suppression of two major fragile X syndrome mouse model phenotypes by the mGluR5 antagonist MPEP. Neuropharmacology. 2005;49:1053–66.
75. Dölen G, Osterweil E, Rao BS, Smith GB, Auerbach BD, Chattarji S, et al. Correction of fragile X syndrome in mice. Neuron. 2007;56:955–62.
76. de Vrij FM, Levenga J, van der Linde HC, Koekkoek SK, De Zeeuw CI, Nelson DL, et al. Rescue of behavioral phenotype and neuronal protrusion morphology in Fmr1 KO mice. Neurobiol Dis. 2008;31:127–32.
77. Berry-Kravis EM, Lindemann L, Jønch AE, Apostol G, Bear MF, Carpenter RL, et al. Drug development for neurodevelopmental disorders: Lessons learned from fragile X syndrome. Nat Rev Drug Discov. 2018;17:280–99.
78. Trubetskoy V, Pardiñas AF, Qi T, Panagiotaropoulou G, Awasthi S, Bigdeli TB, et al. Mapping genomic loci implicates genes and synaptic biology in schizophrenia. Nature. 2022;604:502–8.
79. Ledonne A, Mercuri NB. On the modulatory roles of neuregulins/ErbB signaling on synaptic plasticity. Int J Mol Sci. 2019;21:275.
80. Mei L, Nave KA. Neuregulin-ERBB signaling in the nervous system and neuropsychiatric diseases. Neuron. 2014;83:27–49.
81. Kaphzan H, Hernandez P, Jung JI, Cowansage KK, Deinhardt K, Chao MV, et al. Reversal of impaired hippocampal long-term potentiation and contextual fear memory deficits in Angelman syndrome model mice by ErbB inhibitors. Biol Psychiatry. 2012;72:182–90.
82. Sharghi S, Flunkert S, Daurer M, Rabl R, Chagnaud BP, Leopoldo M, et al. Evaluating the effect of R-Baclofen and LP-211 on autistic behavior of the BTBR and Fmr1-KO mouse models. Front Neurosci. 2023;17:1087788.
83. Namba H, Okubo T, Nawa H. Perinatal exposure to neuregulin-1 results in disinhibition of adult midbrain dopaminergic neurons: implication in schizophrenia modeling. Sci Rep. 2016;6:22606.
84. Aishworiya R, Valica T, Hagerman R, Restrepo B. An update on psychopharmacological treatment of autism spectrum disorder. Neurotherapeutics. 2022;19:248–62.
85. Kalueff AV, Stewart AM, Song C, Berridge KC, Graybiel AM, Fentress JC. Neurobiology of rodent self-grooming and its value for translational neuroscience. Nat Rev Neurosci. 2016;17:45–59.
86. Caldwell-Harris CL. An explanation for repetitive motor behaviors in autism: facilitating inventions via trial-and-error discovery. Front Psychiatry. 2021;12:657774.

ACKNOWLEDGEMENTS

This work was partially supported by Il Fulcro Foundation (AL) and MNESYS (PE0000006)—A Multiscale integrated approach to the study of the nervous system in health and disease (DN. 1553 11.10.2022) (AL, NBM, CB). CB group work was also supported by Telethon Foundation GGP20137, PRIN 20227JA8R3 MUR Next Generation EU and SNSF 310030—215706.

AUTHOR CONTRIBUTIONS

SLD performed mouse surgeries and intracerebral drug injections; performed and analyzed behavioral experiments. ER performed and analyzed western blot experiments. MMC performed and analyzed immunofluorescence experiments. CB supervised western blot experiments. NBM provided devices and resources. AL conceived the project, designed the experiments, performed and analyzed all electrophysiological recordings, dissected brain samples for western blot and immunofluorescence experiments, supervised the project, prepared the figures, and wrote the manuscript. All authors discussed the results, commented on the manuscript and approved the final version.

COMPETING INTERESTS

The authors declare no competing interests.

ADDITIONAL INFORMATION

Supplementary information The online version contains supplementary material available at https://doi.org/10.1038/s41380-024-02831-y.

Correspondence and requests for materials should be addressed to Ada Ledonne.

Reprints and permission information is available at http://www.nature.com/reprints

Publisher's note Springer Nature remains neutral with regard to jurisdictional claims in published maps and institutional affiliations.